Journal of the Taiwan Institute of Chemical Engineers 165 (2024) 105777

Contents lists available at ScienceDirect

Journal of the Taiwan Institute of Chemical Engineers

journal homepage: www.journals.elsevier.com/journal-of-the-taiwan-institute-of-chemical-engineers

Molecular dynamics method to investigate the interaction energy and mechanical properties of the reinforced graphene aerogel with paraffin as the phase change material in the presence of different external heat fluxes

Mostafa Yazdani, Aazam Ghassemi *, Mohamad Shahgholi *, Javad Jafari Fesharaki, Seyed Ali Galehdari

Department of mechanical engineering, Najafabad Branch, Islamic Azad University, Najafabad, Iran.

A R T I C L E I N F O

Keywords:
External heat flux
Graphene aerogel
Phase change material
Molecular dynamic simulation
Composite

A B S T R A C T

Background: Graphene aerogels (GA), known for their exceptional lightweight and sturdy characteristics, present a promising avenue for improving thermal energy (TE) storage and transfer efficiency. It might be possible to make better thermal management systems in fields like electronics, aerospace, and energy storage by studying how heat flux (HF) affects the strength and stability of graphene aerogels.

Methods: The study used molecular dynamics (MD) simulation to investigate how the mechanical properties of graphene aerogels strengthened with paraffin as phase change material (PCM) change in response to external heat flux (EHF). These simulation methods provided a detailed view of molecular interactions and dynamics at the atomic level, allowing researchers to understand the behavior of materials under various conditions. The change in toughness, interaction energy (IE), Young's modules (YM), and ultimate strength (US) was examined for this reason.

Significant findings: The results indicate that when the HF increased from 0.1 to 0.3 W/m^2, the ultimate strength and Young's modules increased from 8.91 and 5.37 GPa to 14.546 and 8.59 GPa, respectively. These values declined when HF increased by more than 0.3 W/m^2. When EHF went up to 0.3 W/m^2, these graphene aerogel properties went up. This was because the atoms moved around more and there were more bonding contacts among the graphene sheets, which made the structure of material stronger. However, at heat flux levels exceeding 0.3 W/m^2, excessive thermal energy may lead to thermal degradation, causing bond breakage and loss of structural integrity, ultimately resulting in a decrease in these mechanical properties. Also, the results reveal that interaction energy increased from -1522.098 to -1546.325 eV as external HF increased to 0.3 W/m^2. The thermal motion of atoms enhanced as the HF increased, enabling closer clustering and better alignment of graphene sheets, thereby strengthening their interactions. This study gave us useful information about how to improve the mechanical properties of graphene aerogels in different HF conditions. This made it more likely that these materials can be used in energy storage systems and thermal management.

1. Introduction

Graphene aerogel (GA) is a porous substance consisting of graphene layers held together by van der Waals forces and chemical bonds [1]. It is extremely lightweight, possesses a substantial surface area, and exhibits excellent electrical conductivity. The main focus of research on GAs was their manufacturing process and their exceptional qualities in experimental conditions. The structure of GA, consisting of one or more graphene layers, is distinct from the connected particles found in traditional aerogels, such as carbon and silica aerogels [2-4]. GAs are formed by bonding graphene sheets together with chemical bonds, adhering closely to each other, and supported by the overall structure. The twisting, bending, and buckling of graphene sheets consistently occur, leading to curved shapes. Although these structures can become unstable and deform under pressure, they are adept at returning to their original shape[5,6]. The curved GA sheets contain numerous breaks due to insufficient condensation reactions during the preparation process [7]. Phase change materials (PCMs) possess many beneficial properties,

* Corresponding author.
E-mail addresses: a_ghassemi@pmc.iaun.ac.ir (A. Ghassemi), M.shahgholi@pmc.iaun.ac.ir (M. Shahgholi).

https://doi.org/10.1016/j.jtice.2024.105777
Received 6 May 2024; Received in revised form 15 September 2024; Accepted 17 September 2024
Available online 26 September 2024

such as high energy density capacity, non-toxicity, and chemical stability. Moreover, PCMs can store or release a significant amount of latent heat within a narrow temperature (Temp) range as they transition from one state to another [8,9]. By adding materials like metal nanoparticles, carbon black, carbon nanotubes, graphite, graphene, graphene oxide, and boron nitride, PCMs may improve their heat conductive capabilities [10,11]. By integrating PCM paraffin with GA, which has excellent mechanical properties and low density, the expectation is to enhance the TE storage capacity while maintaining or improving the structural integrity of the composite material [12,13]. Also, the use of GA as a supporting skeleton for PCMs plays the role of complete encapsulation and improves the mechanical properties of the structure [14].

Baimova et al. [15] conducted research that utilized MD simulations to investigate the strength of various shapes of GAs. In the early stages of bending, the honeycomb cell walls were discovered to be able to move perpendicular to the stress. More pressure causes higher tension in the honeycomb cell connections and tight walls. The length and closeness of honeycombcell walls have a significant effect on GA's efficacy. Scaffaro et al. [16] developed a lightweight GPA material with excellent properties, such as high porosity, a large surface area, biocompatibility, and high strength by incorporating graphene oxide and polyethene glycol. Han et al. [17] developed durable GAs by immersing graphene hydrogels in an ammonia solution. The aerogels are highly durable and can be modified in terms of density and size. The concentration of ammonia in the solution is significant because it directly influences density and volume. As the volume grows, the area shrinks, and the material's walls become more substantial. Zhong et al. [18] produced a unique PCM consisting of 3D graphene and octadecanoic acid (OA). The aerogel was observed via a one-step hydrothermal reaction. The thermal conductivity (TC) of composite material with 20% GA was determined to be 2.635 W m. GA ligaments are capable of preventing liquid leakage in OA which have effective heat transfer capabilities. Wu et al. [19] presented some synthesized GAs with good catalytic that effectively reduce 4-nitrophenol, degrade methyl orange, and purify water contaminated with oil and dye. GAs containing Cu nanoparticles were created by combining and subsequently drying them.

Previous research showed, however, that MD approach was ideal for studying the atomic, thermal, and mechanical behavior of many structures. For example, Noorian et al. [20] investigated how checker surface roughness on the lower wall of nanochannels affects liquid argon flow using MD simulation. Results indicate that increased surface attraction energy and roughness height enhance density layering near the wall, leading to secondary layering phenomena. Xu and Song [21] explored the thermal transport properties of gas-filled silica aerogels via MD simulations. The TC of these composite materials was primarily affected by gas-phase TC in relation to Temp, as indicated by their findings. Conversely, the strain response was primarily affected by changes in the solid-phase TC. Song and Lu [22] utilized MD simulations to examine the microscopic mechanisms of ice melting triggered by laser energy deposition. In particular, this study examined the effects of strain, Temp, gas doping, laser parameters, and laser parameters on melting duration in the Laser Melting and Thermal Transport Melting zones. The results show that melting in the thermal transport melting area was mainly accelerated by Temp increases. Furthermore, in both the transport melting and laser melting regions, the melting process was accelerated by increased laser energy density. Song et al. [23] investigated the thermal transport properties of composite sulfur cathode materials and phase change materials made from GAs using MD simulations. Their experimental data suggested that the theoretical analytical model closely corresponded to MD results, especially when the filler concentrations were larger. Yan et al. [24] focused examining how varying boundary wall Temps (84 K to 133 K) affected Argon fluid flow properties in microchannels with roughened and smooth surfaces. The results suggested that the presence of surface roughness hindered the migration of Argon atoms towards the center of channel and decreased the average fluid velocity by 1% to 3%. However, higher Temps improved boiling, therefore counteracting the effect of roughness phenomena. Jolfaei et al. [25] focused the thermal properties of DNA using equilibrium and non-equilibrium MD, yielding TC values of 0.381 W/m K and 0.373 W/m K, respectively. The results show that TC was determined by the amount of DNA molecules and the equilibrium Temp, which was consistent with previous studies. Toghraie et al. [26] focused the Couette and Poiseuille flows of Water-Copper nanofluids in rough and smooth nanochannels using the MD method. The results show that nanoparticles interacted with the channel surfaces and cause oscillations in the middle region of the fluid. However, making the channel taller lessened the effect of the surfaces on the flow and speed of fluid. Zarringhalam et al. [27] focused the effects of cone-shaped surface roughness on the boiling flow behavior of Argon fluid in microchannels at various boundary wall Temps (84 to 133 K). The results show that while roughness enhanced energy transfer and Temp profiles, it reduced fluid flow velocity by 0.5–1.5%, suggesting that extremely smooth surfaces may not be necessary for practical applications like medical micro probes.

Understanding the functionality of GA is crucial for the development of stretchy electronics, wearable devices, and smart factories. Some disadvantages of GA include volume shrinkage and structural distortion, resulting in reduced strength [28]. The choice of MD simulations is primarily due to the method's ability to provide detailed insights into atomic-level interactions and dynamic behavior over time [29]. MD simulations are well-suited for capturing the complex interplay between thermal and mechanical properties at the nanoscale [30,31], allowing researchers to observe how changes in Temp and energy affect structural integrity, ultimate strength (US), Young's modulus (YM), toughness, and IE. This level of detail is often unattainable with macroscopic methods or continuum models, which may overlook critical molecular interactions. MD can accurately model the behavior of materials at the atomic level; it is computationally intensive and may require significant resources, especially for large systems or long simulation times [32,33]. The mechanical properties of reinforced GA by paraffin as PCM at different external heat fluxes (EHFs) were studied using MD simulation. For this purpose, the change in the US, YM, toughness, and IE variation were investigated.

2. Simulation methods

2.1. Simulation details

This research aimed to examine the effect of EHF on the mechanical behavior of GA reinforced with PCM in a cube simulation box. LAMMPS allowed us to assess the computer's performance. The diagrams in Fig. 1 and Fig. 2 depict the model structure at the first time step. VMD software was utilized to simulate the graphene nanosheet, while the Avogadro software was used to represent oxygen particles and paraffin as PCM. LAMMPS software creates a model of GA's shape. To model GA, first raise the structure's Temp from 300 to 450 K, then drop it to 0 K after 2 ns. Nose-Hoover thermostat will be used in the study to oversee Temp changes in MD simulations of atoms. The organization of modelled structures can be managed using the PACKMOL software after they have been created. Next, the paraffin structure was modelled using Avogadro and added to the GA structure (See Fig.3). Nose-Hoover thermostat is utilized to maintain a constant Temp in simulated atomic structures. Alternatively, the simulation will run for 200000-time steps. After constructing a model of the structure, the equilibrium in the modelling structure is checked. At this point, the NVT ensemble is being used (Table 1).

2.2. The equilibration processes

It is important to confirm that the results obtained from the MD method correspond to the designated simulation time. Temp and kinetic energy (KE) will be used to investigate how atom-by-atom changes affect

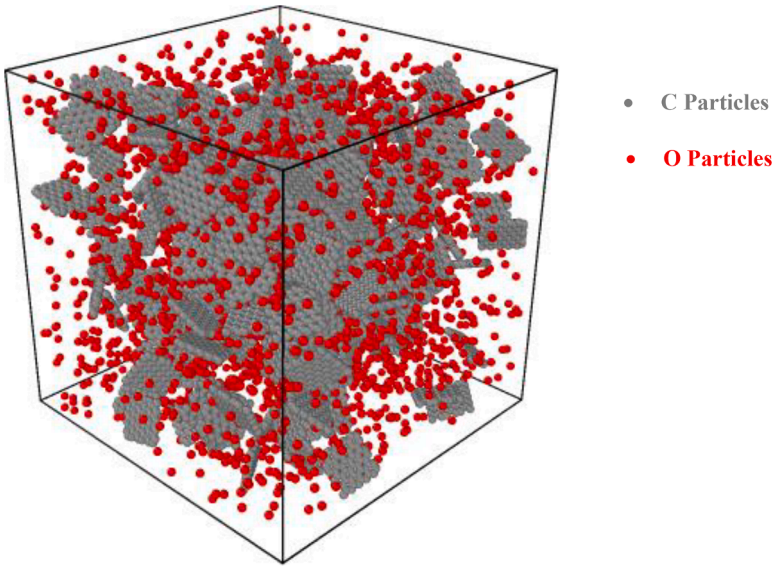

Fig. 1. A schematic of modelled GA in the first-time steps from a perspective view.

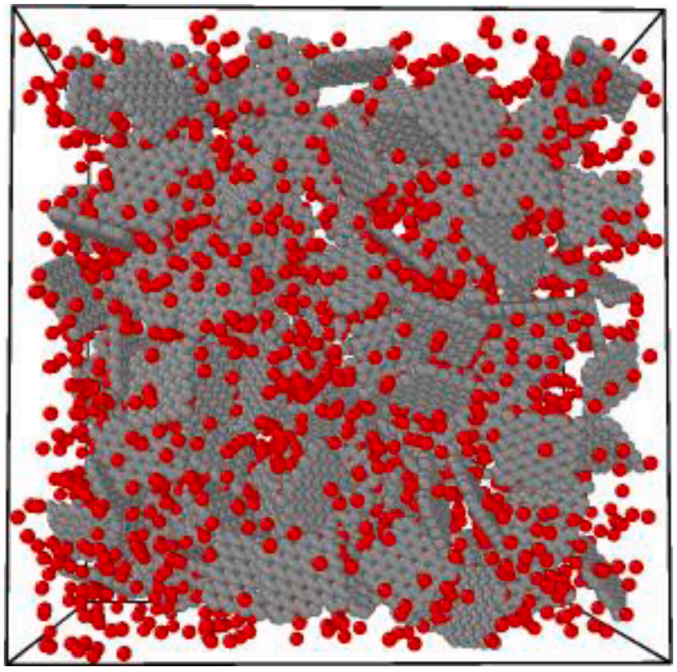

Fig. 2. A schematic of modelled GA in the first-time steps from the side view.

samples. Fig. 4 shows the Temp changes in the simulated atomic composition. The data indicates that this quantity reaches 300 K after 200000-time steps. Under certain conditions, when the vibration of atoms decreases, and their movement becomes more uniform, the Temp will get closer to 300 K. In conclusion, it can be stated that the atoms in the defined samples have retained their positions, and the structure is stable at the initial Temp of 300 K.

Changes in an object's KE within a composite sample can also serve as an indicator of its stability. The data presented in Fig. 5 illustrates the compound's KE variation over time. A number of variables can affect how accurately an MD simulation predicts KE. These variables include the force field's parameters, the dimensions and composition of system being studied, and the frequency of simulation updates. After 200000-time steps, the data indicated that the KE converged to 12.28 eV. Our gathering WAS due to a decrease in atomic movement within the

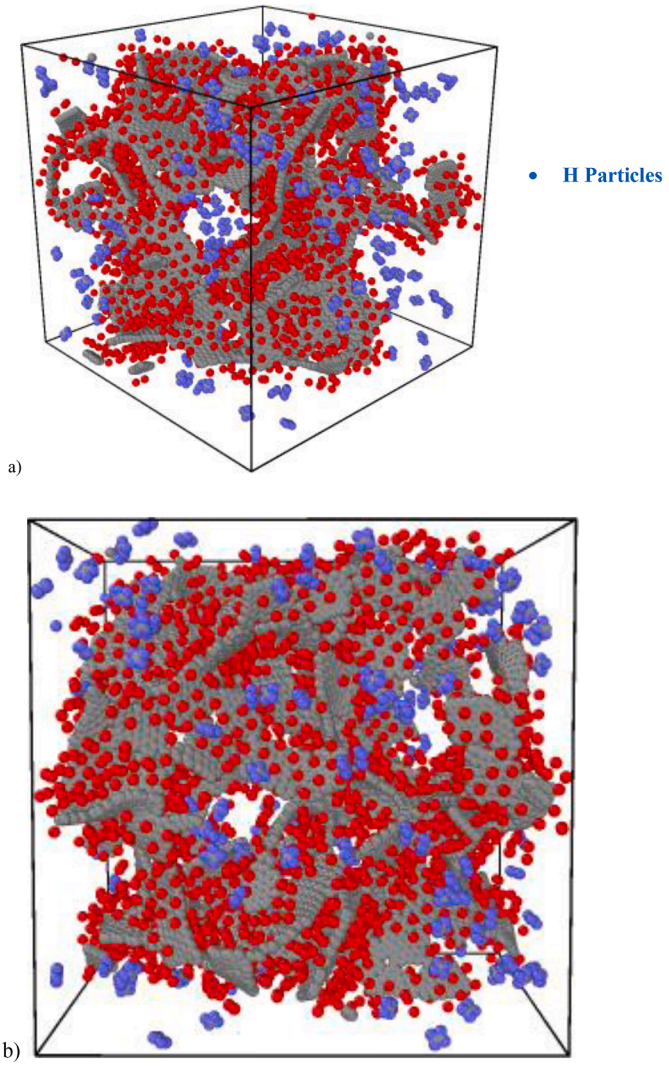

Fig. 3. A schematic of modelled GA /paraffin nanostructure from a) perspective and b) side view.

Table 1
The MD simulation details in the present study.

Parameter	Ratio/Setting
Computational Box Length	100 ×100 ×100 Å^3
Boundary Condition	P P P
Thermostat	Nose-Hoover
MD Simulation Algorithm	NVT/NPT
Initial Temp	300 K
Initial Pressure	1 bar
Time Step	0.2 fs
Number of Simulation Timesteps (Equilibrium Phase)	200,000

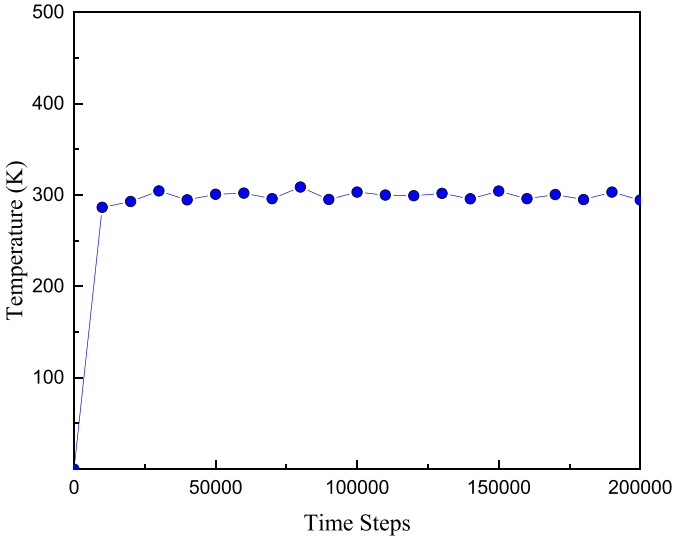

Fig. 4. Temp changes with respect to time steps in the reinforced GA.

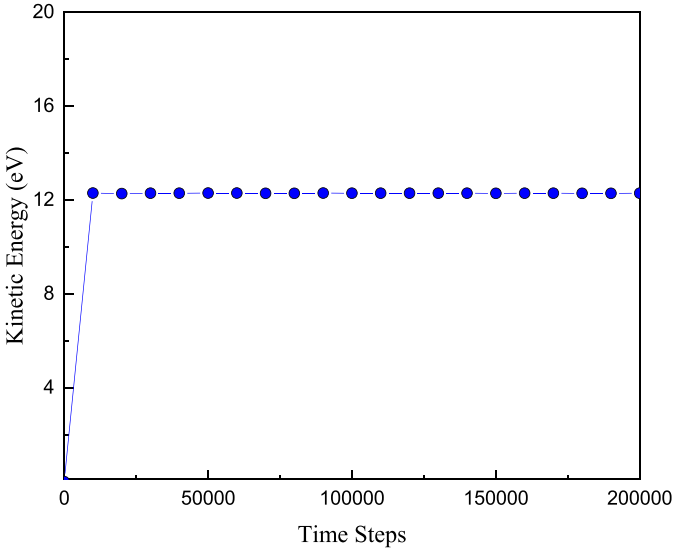

Fig. 5. KE changes with respect to simulation time in the reinforced GA.

simulation box. The simulation demonstrated that our approach to setting it up, such as our modelling of atomic structure and the use of force fields, was suitable. In conclusion, after evaluating our findings from this simulation phase (equilibrium phase) against earlier studies [40-43], we determined that our MD configurations were effectively applied, thereby confirming the validity of our current simulation methodology [44-48].

3. Results

The mechanical test settings were established after the sample reached equilibrium. The simulated GA's YM and US were analyzed in relation to the variations in EHF in the range of 0.1, 0.2, 0.3, 0.4, 0.5, and 1 W/m^2. The stress-strain curve illustrates the behavior of a material under stress. The results of the simulations are depicted in Fig. 6a. It was determined that the strength of reinforced GA decreased as the strain ratio increased. Numerically, the US of reinforced GA reached 8.91 GPa. This parameter represented the maximum (Max) amount of pressure a material can withstand before it failed. It played a critical role in engineering design. Altering YM estimation can provide a more comprehensive understanding of modeled structure's mechanical performance. YM measures a material's ability to withstand resistance to deformation. YM measures a material's ability to with stand resistance to deformation. It is the determination of a material's ability to stretch under applied stress. The numerical value for this mechanical constant can be observed as 5.37 GPa in Fig. 6b.This figure is the indicative of the practicality of using reinforced GA. The obtained results were verified with the results of Patil et al. [49]. They also showed that the US value of GA with different densities is in the range of 8 to 12 GPa.

The toughness is a measure of how much energy the material can

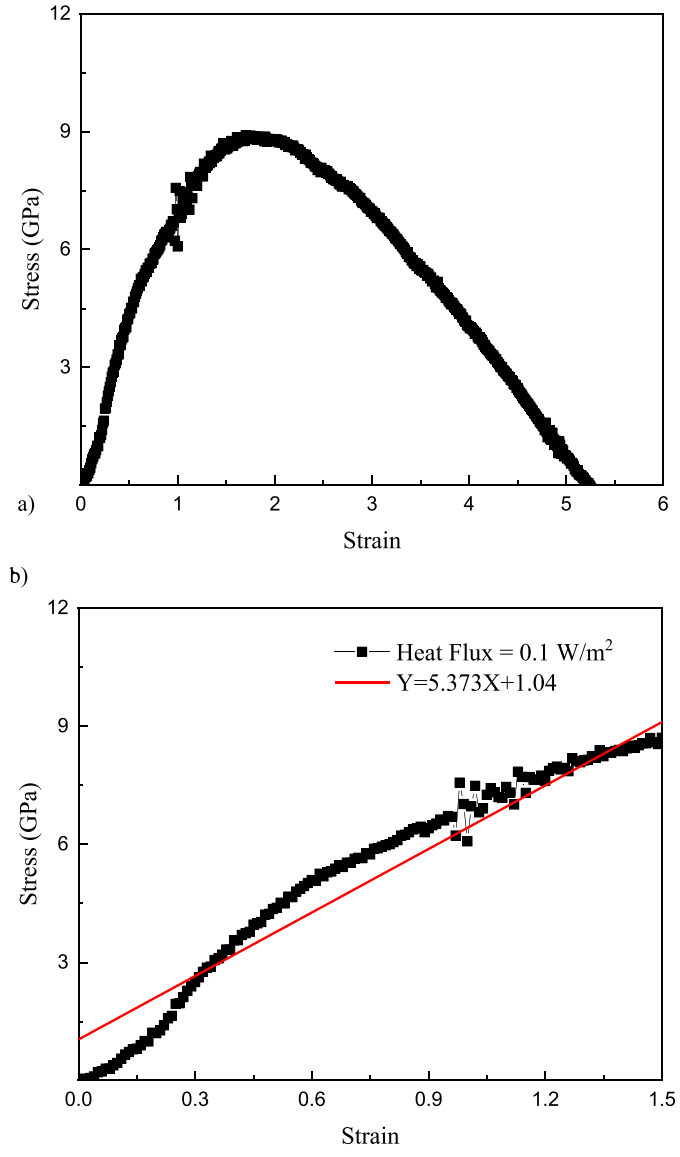

Fig. 6. The a) Stress-strain curve and b) YM of simulated reinforced GA.

absorb before it breaks. In simplified terms, toughness is a measure of a material's capacity to undergo stress and deformation without experiencing failure. The material's capacity to absorb energy prior to failure is quantified by the area under the stress-strain curve. The stress-strain curve illustrates the relationship between stress (force per unit area) and strain (deformation) during loading. The larger the area under the curve, the tougher the material, indicating it can withstand more stress and deformation before breaking. This calculation provides a quantitative measure of the material's resilience and durability. Fig. 7 shows a graph that illustrates this toughness, helping to evaluate the material's mechanical properties and total performance under various conditions. Numerically, this parameter converged to 24.24 eV/Å^3.

IE is the portion of total energy that is a result of the interaction among the objects under consideration. IE is typically determined by the relative positions of objects. The IE was affected by increased mobility of particles within the sample as a result of the administration of EHF. Numerically, Max amount of IE per atom of reinforced GA reached 29.33 eV, as shown in Fig. 8.

The particles were in motion within the sample as a result of EHF. The change in the US of reinforced GA at various EHFs is illustrated in Fig. 9. According to our model, changes in these parameters significantly affect the US of reinforced GA, as shown in Fig. 9. US increased from the numerical value of 8.91 to 14.54 GPa as a result of the change in EHF parameter from 0.1 to 0.3 W/m^2. Hence the US increased to 14.54 GPa at a heat flux of 0.3 W/m^2. The increase in US of EHF-reinforced GA from 0.1 to 0.3 W/m^2 can be attributed to the increased atomic mobility and improved bonding interactions among graphene sheets, which strengthen the structure of material. When the EHF increased initially, it can increase the thermal activation of GA material. This led to a better bond between the graphene and the paraffin and improves total mechanical properties, such as US. The thermal flux and as a result the heat helped reduce the brittleness and increase the ductility of material in question which allowed it to withstand mechanical stress better without breaking. However, due to the further increase of the EHF and reaching the value of 1 W/m^2, the excessive TE may lead to thermal degradation, causing bond breakage and loss of structural integrity. Finally, it resulted in a reduction of US, reaching a numerical value of 7.89 GPa. The stability of atomic structures was significantly affected by atomic vibrations and oscillations, particularly in GA materials with high HFs. High EHF caused an increase in Temp and TE in nanostructured materials. This resulted in the atoms vibrating more violently, which can impair the bonds that maintained the atomic structure. This can result in bond stretching and possible breakage. This behavior highlighted the delicate balance between beneficial thermal activation and detrimental thermal effects.

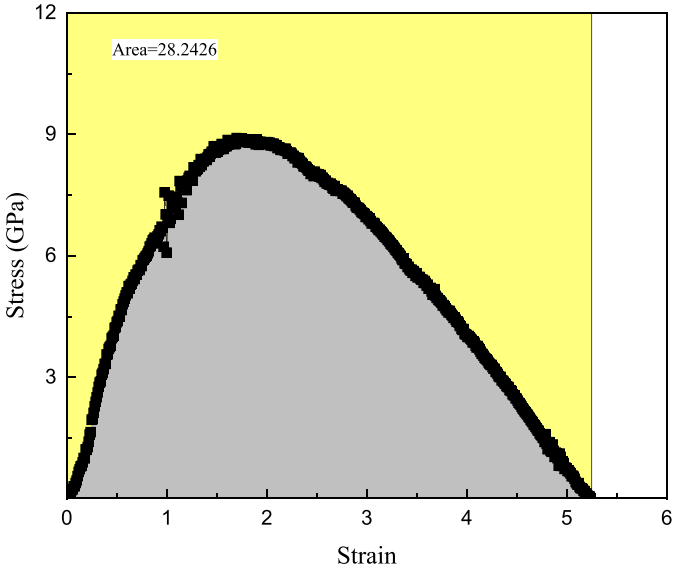

Fig. 7. The toughness of the reinforced GA sample at EHF=0.1 W/m^2.

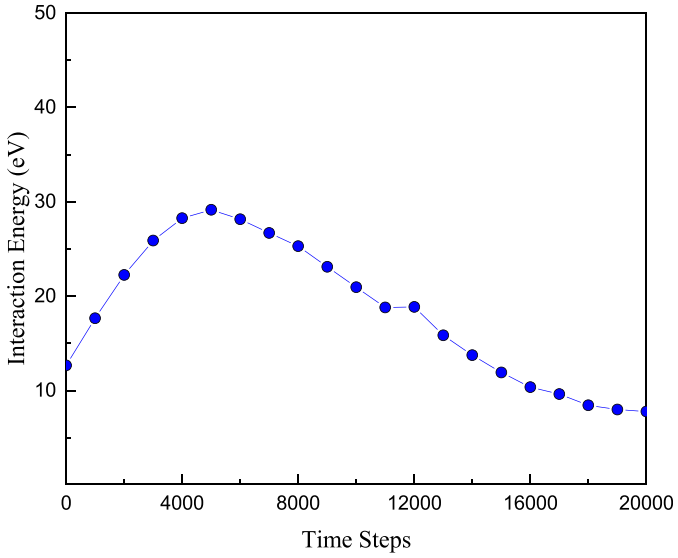

Fig. 8. The IE of simulated reinforced GA at EHF=0.1 W/m^2.

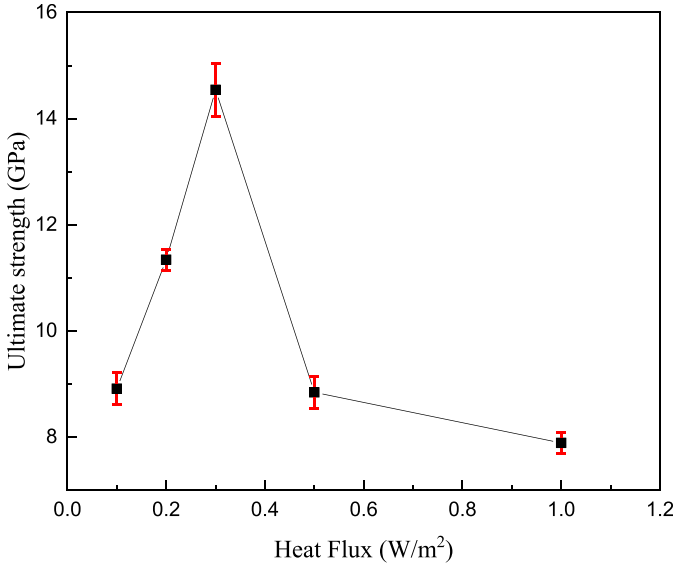

Fig. 9. The US of the simulated reinforced GA sample at different EHFs.

The changes in the YM of reinforced GA at various EHFs are illustrated in Fig. 10. The results show that the presence of EHF in the box improved the stability and cohesion of sample atoms. YM achieved its optimum at 8.59 GPa under an EHF of 0.3 W/m^2, as illustrated in Fig. 10. With the further increase of EHF and reaching the numerical value of 1 W/m^2, the physical parameter of YM decreased to 4.79 GPa. The relationship between YM and EHF in reinforced GAs highlighted how TE affected the material's mechanical properties. At an optimal EHF of 0.3 W/m^2, TE enhances atomic mobility, allowing atoms to vibrate more freely and facilitating better alignment and bonding among the graphene sheets. This improved cohesion and structural integrity result in a Max YM of 8.59 GPa, indicating that the material can withstand greater stress without deforming. Therefore, there was an optimal range of HF where the mechanical properties maximized. This was because moderate heat can facilitate the phase change of paraffin material, increasing its ability to absorb and dissipate energy. A more

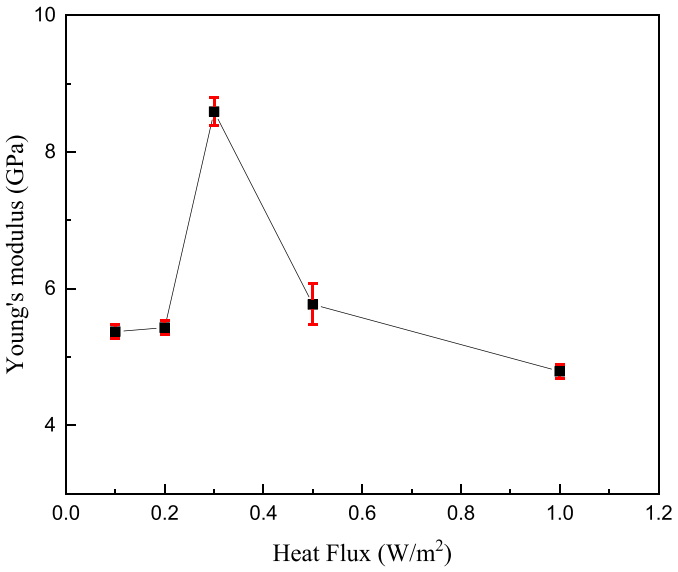

Fig. 10. The YM of the simulated reinforced GA sample at different EHFs.

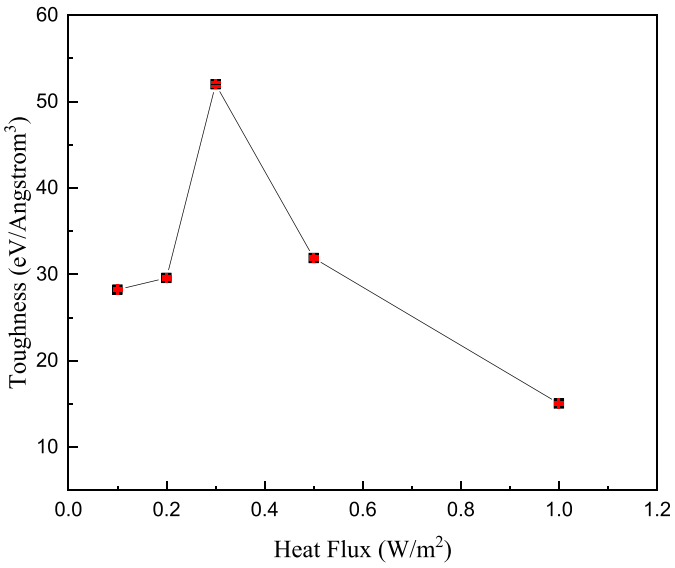

Fig. 11. The toughness of simulated reinforced GA sample at different EHFs.

uniform material structure and enhanced surface adherence were factors in better mechanical performance. The total stiffness and robustness of material were a result of the enhanced bonding interactions at this level of EHF. Furthermore, melting or softening of paraffin phase in the GA might result from excessive EHF. Paraffin may aid in the reorganization of its molecular structure as it transitions from a solid to a more fluid condition. This process can increase the crystallinity after cooling, resulting in a more organized and stable structure that helped improve mechanical strength and thermal stability. However, as the EHF increased beyond 0.3 W/m^2, the YM began to diminish. At higher EHF levels, such as 1 W/m^2, excessive TE can lead to thermal degradation, disrupting the atomic structure and weakening the bonds among graphene sheets. From a physical point of view, the increase in HF caused the atoms to vibrate more intensely and the bonds that held the atomic structure weakened, eventually leading to bond stretching and possible breakage. Furthermore, increasing the HF concentration may cause microstructural changes in the aerogel, such as pore collapse or a shift in pore size distribution. These variations may have an effect on how stress was distributed throughout the material, possibly resulting in unequal stress concentrations, bond failure, and a decreased YM of structure. The balance between beneficial thermal activation and detrimental thermal effects was crucial, as too much heat can introduce thermal stress and microstructural damage, ultimately compromising the material's mechanical performance.

Fig. 11 represents the change in the toughness of reinforced GA at different EHFs. The results reveal that the toughness increased from 28.24 to 52.01 eV/Å^3 by increasing EHF from 0.1 to 0.3 W/m^2. With further increasing of EHF to more than 0.3 W/m^2, these quantities decreased. The toughness of reinforced GA increased when the EHF increased to 0.3 W/m^2. As EHF increased, the vibrational energy of molecules inside the paraffin and the structure of GA increased. This increased vibrational energy can lead to greater molecular mobility, allowing the polymer chains in the paraffin to rearrange and withstand stress better. The interfacial bonding between paraffin and graphene can be enhanced by improved molecular mobility, which resulted in a more cohesive material that can absorb more energy before breaking. This issue led to an increase in durability. Moreover, HF had the potential to affect the crystal structure of graphene, which could result in enhanced crystallinity or an alignment of the graphene sheets. By facilitating more effective load transfer through the material, a well-aligned crystal structure can improve mechanical properties, such as durability. However, when the EHF increased from 0.3 to 1 W/m^2, the toughness decreased from 52.01 to 15.05 eV/Å^3. At very high EHF levels, excessive vibrational energy can lead to thermal degradation of paraffin and changes in graphene structure. This degradation can weaken the material and reduce the ability to absorb energy and lead to a decrease in toughness. Also, high Temp can cause disturbances in the crystalline structure of graphene, cause defects or disrupt the arrangement of graphene layers. These defects can act as stress concentrators, leading to premature failure and reduced toughness. Essentially, while moderate heat improved the material, too much heat caused damage, resulting in a loss of mechanical integrity.

The Max amount of IE per atom changes in reinforced GA indicated in Fig. 12. According to the simulation results, IE reached its Max value of 38.73 eV due to the application of EHF of 0.3 W/m^2. Then, by further increasing the EHF and reaching the numerical value of 1 W/m^2, the IE decreased to 18.59 eV. The increase in IE with increasing EHF ratio can be attributed to the increase in atomic and bonding interactions because the input energy optimized the structural arrangement of atoms. As a consequence of elevated EHF, the molecular vibrations and motions within paraffin-reinforced GA material were stimulated by the availability of energy. This thermal stimulation had the potential to enhance

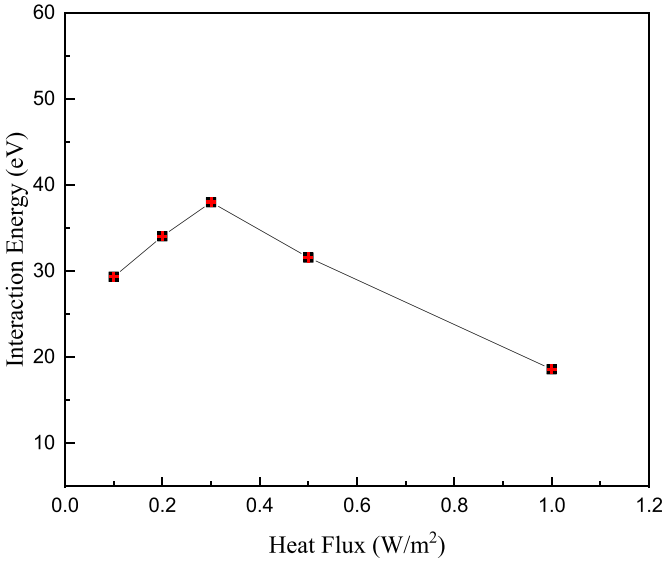

Fig. 12. IE of simulated reinforced GA as a function of EHF.

intermolecular forces, including hydrogen bonding and van der Waals interactions, resulting in an increase in IE. Additionally, the compatibility between GA and paraffin can be enhanced by higher EHFs, which resulted in improved interfacial interactions and, as a result, an increase in the total IE. However, when the EHF increased to 1 W/m^2, the interaction energy decreased to 18.59 eV due to several physical factors. Excess energy can lead to an increase in the KE of molecules and atomic vibrations, as well as disrupt stable bond configurations, resulting in weaker and less effective interactions. This was due to the decreased likelihood of molecules staying in close proximity. Besides, higher energy levels may induce phase changes, potentially moving the material into a less ordered state, which typically had a lower IE. The probability of bond dissociation increased with excess energy, which contributed to observed decrease in interaction energy as the system becomes less stable.

The US, YM, toughness, and IE parameter values can be found in Table 2. The study revealed that GA has multiple potential uses and can offer a range of strength capabilities. Excessive EHF can disturb the atomic organization and lead to repulsion among them. As a result, the sample will shatter, and its mechanical properties will be diminished. Designers and engineers need to contemplate. Among various studies [50-52] reported the substance's mechanical properties, the present article applied a MD computer simulation to assess the effect of EHF application on the mechanical strength of GA reinforced by PCM.

4. Conclusions

Our research involved utilizing a computer simulation to assess the effect of EHF application on the mechanical strength of GA reinforced by PCM. In the preliminary step of equilibration process, simulations were performed and yielded these outcomes:

- After 200000-time step, Temp and KE converged to 300 K and 12.28 eV, according to the results. This convergence signified that the system reached a stable equilibrium state, where thermal fluctuations and energy configurations were balanced, allowing for accurate simulation of material properties.

An EHF was introduced to the equilibrated sample, and the following results were derived from this part of simulation:

- When EHF increased from 0.1 to 0.3 W/m^2, US and YM increased from 8.91 and 5.37 GPa to 14.546 and 8.59 GPa, respectively. When EHF increased to 1 W/m^2, these quantities decreased to 7.89 and 4.79 GPa, respectively.
- Toughness increased from 28.24 to 52.01 eV/Å^3 by increasing EHF to 0.3 W/m^2. With further increases of EHF more than 0.3 W/m^2, these quantities decreased. The toughness of reinforced GA increased when EHF increased to 0.3 W/m^2 because this level of TE enhanced atomic interactions and bonding within the material.
- The MD results indicated that the IE of sample varied from 29.33 to 38.73 eV with increasing EHF to 0.3 W/m^2. By further increasing EHF to 1 W/m^2, these quantities decreased to 18.59 eV.

Funding

There is no funding.

CRediT authorship contribution statement

Mostafa Yazdani: Writing – review & editing. **Aazam Ghassemi:** Writing – review & editing. **Mohamad Shahgholi:** Writing – review & editing. **Javad Jafari Fesharaki:** Writing – review & editing. **Seyed Ali Galehdari:** Writing – review & editing.

Declaration of competing interest

The authors declare that they have no known competing financial interests or personal relationships that could have appeared to influence the work reported in this paper.

Appendix

A. MD simulation

The use of MD simulation is critical for investigating the assembly and function of biological molecules [34]. MD entails using a computer simulation to demonstrate how particles interacted and moved in accordance with physics principles. MD simulation entails solving Newton's motion equations. The movement of all particles over time can be simulated by solving these equations [32]. In MD simulations, it is crucial to consider how the potential function and forces among the particles are established. The potential function is typically categorized into bonded and non-bonded potentials [35]. The total potential energy of a system is determined by calculating the combined effects of particle interactions within the system [36].

$$E_{total} = E_{bonded} + E_{nonbonded} \quad \text{(a-1)}$$

Different types of potential energy arise from non-bonded interactions when discussing non-bonded potentials. Lennard-Jones potential function is a fundamental mathematical equation used to predict the interaction between two neutral particles or molecules [37]. The most common relation of Lennard-Jones potential function is in the form of Eq. a-2.

$$U_{LJ} = 4\varepsilon_{ij}\left[\left(\frac{\sigma_{ij}}{r_{ij}}\right)^{12} - \left(\frac{\sigma_{ij}}{r_{ij}}\right)^{6}\right] r < r_c \quad \text{(a-2)}$$

In Eq.a-2, ε_{ij} is the depth of the potential well of finite distance where the potential function became zero and the distance of the particles from each other. On the other hand, r_c indicates the cut-off radius in simulated samples, the average value of which is equal to 12 Å in many reports.

In the MDS, two methods of equilibrium dynamics and non-equilibrium dynamics were utilized to determine thermal attributes. Non-equilibrium simulation is less accurate than the equilibrium method. Therefore, the alternative method for the non-equilibrium method is the equilibrium method. No Temp difference was applied to the system in the equilibrium simulation, but the prediction of particle movement and vibration was utilized to determine the temp. attributes.

Table 2
The US, YM, Toughness, and IE variation of reinforced GA as a function of EHF.

EHF (W/m^2)	Max IE (eV)	US (GPa)	YM (GPa)	Toughness (eV/Å^3)
0.1	29.33 (±0.02)	8.91 (±0.3)	5.37 (±0.1)	28.242 (±0.15)
0.2	34.04 (±0.01)	11.34 (±0.2)	5.43 (±0.1)	29.59 (±0.21)
0.3	38. 73 (±0.03)	14.54 (±0.5)	8.59 (±0.2)	52.01 (±0.23)
0.5	31.57 (±0.02)	8.84 (±0.3)	5.77(±0.3)	31.89 (±0.17)
1.0	18.59 (±0.01)	7.89 (±0.2)	4.79 (±0.1)	15.058 (±0.13)

This type of thermal calculation can be performed using the Green-Kubo formulation. This type of formulation calculates the thermal attributes utilizing the following Eqs. [38,39]:

$$K = \frac{V}{3k_B T^2}\int_0^{\infty} dt\langle J(\tau).J(0)\rangle \tag{a-3}$$

In this regard, V is the volume occupied by the particles present in the simulation, kB is Boltzmann's constant, T is the Temp of system, and J is the HF. On the other hand, the term inside the integral refers to the mean of the matching function of the HF. The HF vector is obtained from the following Eq. [38,39]:

$$J = \frac{1}{V}\left[\sum_i e_i v_i - \frac{1}{2}\sum_{i<j}\left(f_{ij}.\left(v_i + v_j\right)x_{ij}\right)\right] \tag{a-4}$$

In the recent formulation, i and j represent two carbon atoms at the two ends of bond, ei denotes the total energy for each particle in the system, vi represents the velocity of particles, S_i represents the entropy of the system, f_{ij} represents the force exerted on the particles of i and j, and V represents the total volume of specimen under investigation. Therefore, by calculating this sigma, the J value of HF flowing in the simulated system is calculated. In this research, HF parameter was chosen between 0.1 and 1 W/m^2. Because in this range, the modeled structure had thermal stability and more reliable results were obtained.

References

[1] Hu H, Zhao Z, Wan W, Gogotsi Y, Qiu J. Ultralight and highly compressible graphene aerogels. Advanced materials 2013;25(15):2219–23.
[2] Worsley MA, Kucheyev SO, Mason HE, Merrill MD, Mayer BP, Lewicki J, Valdez CA, Suss ME, Stadermann M, Pauzauskie PJ. Mechanically robust 3D graphene macroassembly with high surface area. Chemical Communications 2012; 48(67):8428–30.
[3] Lei J, Liu Z, Yeo J, Ng TY. Determination of the Young's modulus of silica aerogels–an analytical–numerical approach. Soft Matter 2013;9(47):11367–73.
[4] Patil SP, Rege A, Sagardas MItskov, Markert B. Mechanics of nanostructured porous silica aerogel resulting from molecular dynamics simulations. The Journal of Physical Chemistry B 2017;121(22):5660–8.
[5] Zhu C, Han TY-J, Duoss EB, Golobic AM, Kuntz JD, Spadaccini CM, Worsley MA. Highly compressible 3D periodic graphene aerogel microlattices. Nat Commun 2015;6(1):6962.
[6] Wang Z, Shen X, Akbari Garakani M, Lin X, Wu Y, Liu X, Sun X, Kim J-K. Graphene aerogel/epoxy composites with exceptional anisotropic structure and properties. ACS Appl Mater Interfaces 2015;7(9):5538–49.
[7] Li C, Shi G. Three-dimensional graphene architectures. Nanoscale 2012;4(18): 5549–63.
[8] Advincula P, De Leon A, Rodier B, Kwon J, Advincula R, Pentzer E. Accommodating volume change and imparting thermal conductivity by encapsulation of phase change materials in carbon nanoparticles. Journal of Materials Chemistry A 2018;6(6):2461–7.
[9] Liu Z, Yu ZJ, Yang T, Qin D, Li S, Zhang G, Haghighat F, Joybari MM. A review on macro-encapsulated phase change material for building envelope applications. Build Environ 2018;144:281–94.
[10] Cao R, Chen S, Wang Y, Han N, Liu H, Zhang X. Functionalized carbon nanotubes as phase change materials with enhanced thermal, electrical conductivity, light-to-thermal, and electro-to-thermal performances. Carbon N Y 2019;149:263–72.
[11] Yang J, Tang L-S, Bao R-Y, Bai L, Liu Z-Y, Yang W, Xie B-H, Yang M-B. An ice-templated assembly strategy to construct graphene oxide/boron nitride hybrid porous scaffolds in phase change materials with enhanced thermal conductivity and shape stability for light–thermal–electric energy conversion. Journal of Materials Chemistry A 2016;4(48):18841–51.
[12] Atinafu DG, Yun BY, Yang S, Yuk H, Wi S, Kim S. Structurally advanced hybrid support composite phase change materials: architectural synergy. Energy Storage Mater 2021;42:164–84.
[13] Zheng X, Gao X, Huang Z, Li Z, Fang Y, Zhang Z. Form-stable paraffin/graphene aerogel/copper foam composite phase change material for solar energy conversion and storage. Solar Energy Materials and Solar Cells 2021;226:111083.
[14] He M, Xie D, Yin L, Gong K, Zhou K. Influences of reduction Temp on energy storage performance of paraffin wax/graphene aerogel composite phase change materials. Mater Today Commun 2023;34:105288.
[15] Baimova JA, Shcherbinin SA. Strength and Deformation Behavior of Graphene Aerogel of Different Morphologies. Materials 2023;16(23):7388.
[16] Scaffaro R, Maio A, Lopresti F, Giallombardo D, Botta L, Bondì ML, Agnello S. Synthesis and self-assembly of a PEGylated-graphene aerogel. Compos Sci Technol 2016;128:193–200.
[17] Han Z, Tang Z, Shen S, Zhao B, Zheng G, Yang J. Strengthening of graphene aerogels with tunable density and high adsorption capacity towards Pb2+. Sci Rep 2014;4(1):5025.
[18] Zhong Y, Zhou M, Huang F, Lin T, Wan D. Effect of graphene aerogel on thermal behavior of phase change materials for thermal management. Solar Energy Materials and Solar Cells 2013;113:195–200.
[19] Wu T, Chen M, Zhang L, Xu X, Liu Y, Yan J, Wang W, Gao J. Three-dimensional graphene-based aerogels prepared by a self-assembly process and its excellent catalytic and absorbing performance. Journal of Materials Chemistry A 2013;1 (26):7612–21.
[20] Noorian H, Toghraie D, Azimian A. Molecular dynamics simulation of Poiseuille flow in a rough nano channel with checker surface roughnesses geometry. Heat and mass transfer 2014;50:105–13.
[21] Xu S, Song J. Thermal transport properties of gas-filled silica aerogels. RSC Adv 2024;14(28):20210–9.
[22] Song J, Lu Y. Atomic-level insights into ice melting induced by femtosecond laser energy deposition. International Communications in Heat and Mass Transfer 2024; 157:107802. 2024/09/01/.
[23] Song J, Xu X, Liang X. Thermal transport properties of graphene aerogel as an advanced carrier for enhanced energy storage. Physical Chemistry Chemical Physics 2024;26(3):2025–34.
[24] Yan S-R, Shirani N, Zarringhalam M, Toghraie D, Nguyen Q, Karimipour A. Prediction of boiling flow characteristics in rough and smooth microchannels using molecular dynamics simulation: Investigation the effects of boundary wall Temps. J Mol Liq 2020;306:112937.
[25] Jolfaei NA, Jolfaei NA, Hekmatifar M, Piranfar A, Toghraie D, Sabetvand R, Rostami S. Investigation of thermal properties of DNA structure with precise atomic arrangement via equilibrium and non-equilibrium molecular dynamics approaches. Comput Methods Programs Biomed 2020;185:105169.
[26] Toghraie D, Hekmatifar M, Salehipour Y, Afrand M. Molecular dynamics simulation of Couette and Poiseuille Water-Copper nanofluid flows in rough and smooth nanochannels with different roughness configurations. Chemical Physics 2019;527:110505.
[27] Zarringhalam M, Ahmadi-Danesh-Ashtiani H, Toghraie D, Fazaeli R. Molecular dynamic simulation to study the effects of roughness elements with cone geometry on the boiling flow inside a microchannel. Int J Heat Mass Transf 2019;141:1–8.
[28] Kong M, Yang M, Li R, Long Y-Z, Zhang J, Huang X, Cui X, Zhang Y, Said Z, Li C. Graphene-based flexible wearable sensors: mechanisms, challenges, and future directions. The International Journal of Advanced Manufacturing Technology 2023:1–33.
[29] Esseiva P, Ioset S, Anglada F, Gasté L, Ribaux O, Margot P, Gallusser A, Biedermann A, Specht Y, Ottinger E. Forensic drug intelligence: an important tool in law enforcement. Forensic Sci Int 2007;167(2-3):247–54.
[30] S. Wenner, "Molecular dynamics simulations of nanoscale mechanical processes," 2010.
[31] Yedla N, Salman SA, Karthik V. Molecular dynamics simulations for nanoscale insight into the phase transformation and deformation behavior of shape-memory materials. Shape Memory Composites Based on Polymers and Metals for 4D Printing: Processes, Applications and Challenges 2022:67–80.
[32] Adcock SA, McCammon JA. Molecular dynamics: survey of methods for simulating the activity of proteins. Chem Rev 2006;106(5):1589–615.
[33] Dong Y, Li Q, Martini A. Molecular dynamics simulation of atomic friction: A review and guide. Journal of Vacuum Science & Technology A 2013;31(3).
[34] Bernardi RC, Melo MC, Schulten K. Enhanced sampling techniques in molecular dynamics simulations of biological systems. Biochimica et Biophysica Acta (BBA)-General Subjects 2015;1850(5):872–7.
[35] Joshi SY, Deshmukh SA. A review of advancements in coarse-grained molecular dynamics simulations. Mol Simul 2021;47(10-11):786–803.
[36] Wu H-J, Bevan MA. Direct measurement of single and ensemble average particle–surface potential energy profiles. Langmuir 2005;21(4):1244–54.
[37] Lennard-Jones JE. Cohesion. Proceedings of the Physical Society 1931;43(5):461.
[38] M. H. Khadem, and A. P. Wemhoff, "Comparison of Green–Kubo and NEMD heat flux formulations for thermal conductivity prediction using the Tersoff potential," vol. 69, pp. 428-434, 2013.
[39] Y. Zheng, X. Zhang, M. T. Soleimani Mobareke, M. Hekmatifar, A. Karimipour, R. J. J. o. T. A. Sabetvand, and Calorimetry, "Potential energy and atomic stability of H 2 O/CuO nanoparticles flow and heat transfer in non-ideal microchannel via molecular dynamic approach: the Green–Kubo method," vol. 144, pp. 2515-2523, 2021.
[40] Sabetvand R, Toghraie D, Hekmatifar M. The molecular dynamics study of boron-nitride nanosheet roughness after atomic bombardment process. J Mol Liq 2021; 331:115733.

[41] Zhao L, Nasution MK, Hekmatifar M, Sabetvand R, Kamenskov P, Toghraie D, Alizadeh Aa, Iran TG. The improvement of mechanical properties of conventional concretes using carbon nanoparticles using molecular dynamics simulation. Sci Rep 2021;11(1):1–12.
[42] Liu Q, Bykanova O, Akhmadeev R, Baghaie S, Hekmatifar M, Arefpour A, Sabetvand R, Borisov V. The numerical study of pressure and Temp effects on mechanical properties of baghdadite-based nanostructure: molecular dynamics simulation. Sci Rep 2022;12(1):1–12.
[43] Shan Liqing, Jasim Dheyaa J, Mohammad Sajadi S, Al-Bayati Alaa Dhari Jawad, Ahmad Nafis, Esfahani Navid Nasajpour, Ridha Benien M, Alsalamy Ali H, Baghaei Sh. Comprehensive analysis of dispersion and aggregation morphology of nanoparticles on the thermophysical properties of water-based nanofluids using molecular dynamics simulation. J Taiwan Inst Chem Eng 2023;150:105043.
[44] Dong Shouliang, Majdi Hasan Sh, Alizadeh As' ad, Thaibat Russul, Hashim Furqan S, Abdullah Hasan Mohammed, Aziz Qusay Husam, Hekmatifar Maboud, Sabetvand Rozbeh. The effect of external force and magnetic field on atomic behavior and pool boiling heat transfer of Fe3O4/ammonia nanofluid: A molecular dynamics simulation. J Taiwan Inst Chem Eng 2023;145:104781.
[45] Salarnia Mohammad, Toghraie Davood, Fazilati Mohammad Ali, Mehmandoust Babak, Pirmoradian Mostafa. The effects of different nanoparticles on physical and thermal properties of water in a copper oscillating heat pipe via molecular dynamics simulation. J Taiwan Inst Chem Eng 2023;143:104721.
[46] Hu Xuefang, Derakhshanfard Amir Hossein, Patra Indrajit, Khalid Imran, Jalil Abduladheem Turki, Opulencia Maria Jade Catalan, Dehkordi Reza Balali, Toghraie Davood, Hekmatifar Maboud, Sabetvand Roozbeh. The microchannel type effects on water-Fe3O4 nanofluid atomic behavior: Molecular dynamics approach. J Taiwan Inst Chem Eng 2022;135:104396.
[47] Tian Wende, Wang Tianshu, Cui Zhe, Zhang Haoran, An Yang. Molecular dynamics and steady-state process simulation coupled research on CCLG system design for cleaner production of EG. J Taiwan Inst Chem Eng 2022;141:104597.
[48] Liang Qian, Valizadeh Kamran, Bateni Amir, Patra Indrajit, Abdul-Fattah Marwa N, Kandeel Mahmoud, Zahra Musaddak Maher Abdul, Bashar Bashar S, Baghaei Shaghayegh, Esmaeili Shadi. The effect of type and size of nanoparticles and porosity on the pool boiling heat transfer of water/Fe nanofluid: Molecular dynamics approach. J Taiwan Inst Chem Eng 2022;136:104409.
[49] Patil SP, Shendye P, Markert B. Molecular investigation of mechanical properties and fracture behavior of graphene aerogel. The Journal of Physical Chemistry B 2020;124(28):6132–9.
[50] Huang Jiali, Wang Xin, Guo Wenwen, Niu Haoxin, Song Lei, Hu Yuan. Eco-friendly thermally insulating cellulose aerogels with exceptional flame retardancy, mechanical property and thermal stability. J Taiwan Inst Chem Eng 2022;131:104159.
[51] AhadiParsa Mobina, Dehghani Ali, Ramezanzadeh Bahram. Titanium carbide-based (Ti3C2) MXene@ Zn-doped-S-polyaniline nanosheets: Toward thermo-mechanical and UV-shielding properties enhancement. J Taiwan Inst Chem Eng 2024;156:105364.
[52] Ghamsarizade R, Ramezanzadeh B, Mohammadloo HEivaz. A review on recent advances in 2D-transition metal carbonitride-MXenes nano-sheets/polymer composites' electromagnetic shields, mechanical and thermal properties. J Taiwan Inst Chem Eng 2023;144:104740.